Revisiting Mulliken's Concepts about Rydberg States and Rydberg−Valence Interactions from Large-Scale Ab Initio Calculations on the Acetylene Molecule†

Fabrice Laruelle,‡ Séverine Boyé-Péronne,§ Dolores Gauyacq,*,§ and Jacques Liévin*,‡

Service de Chimie Quantique et Photophysique, Université Libre de Bruxelles, Cpi 160/09, 50 Av. F.D. Roosevelt, B-1050 Bruxelles, Belgium, and Laboratoire de Photophysique Moléculaire, CNRS UPR 3361, Université Paris-Sud 11, Bât. 210, F-91405 Orsay Cédex, France

Received: April 29, 2009; Revised Manuscript Received: June 23, 2009

A quantitative characterization of the Rydberg and valence singlet electronic states of acetylene lying in the 5−10.7 eV region is performed by using large-scale ab initio calculations. A special attention is paid on the comparison between the present calculations and Mulliken's concepts for Rydberg states, based on single-electron and single-configuration description. Most of the properties of the Rydberg states have been qualitatively understood via this comparison, mainly shown by the shape and size of the outer Rydberg molecular orbital. More quantitatively, Rydberg−valence mixing has been evaluated in several excited energy regions, as for instance, the interaction between the $\tilde{C}'$ $(1\pi_g)^2$ ^1A_g doubly excited valence state and the manifold of electronic components of the *n*p series, or the interaction between the $\tilde{E}$ $1\pi_g$ ^1B_u valence state and the $\tilde{F}$ $3d\pi_g$ $^1\Sigma_u^+$ Rydberg state. The rapid predissociation of the lowest $\tilde{C}$ $3s\sigma$ $^1\Pi_u$ Rydberg state has been interpreted as a case of Rydbergization, earlier predicted by Mulliken.

I. Introduction

Acetylene is a prototype polyatomic molecule for studying large amplitude nuclear motions due to the very labile nature of the H atom. In particular, the vibrational dynamics of this molecule has been extensively studied both experimentally and theoretically by R. W. Field and collaborators (see for instance ref 1 and references therein). In addition to this fundamental aspect, acetylene is a key molecule for the interstellar carbon chemistry and photochemistry.[2−4] Indeed, it is easily ionized or dissociated by the vacuum-ultraviolet (VUV) interstellar radiation giving rise to very reactive species such as the C_2H, CH, and C_2 radicals,[5,6] which in turn enter a complex reaction chain leading to the formation of more complex molecules as polycyclic aromatic hydrocarbons, organic compounds, or soots.

In the laboratory, the VUV spectroscopy and dynamics of acetylene has been extensively studied, both experimentally[6−21] and theoretically.[20,22−26] In the region up to 11 eV, the absorption spectrum of acetylene is dominated by excitation of the singlet Rydberg states which carry the strongest oscillator strength.[27] On the other hand, in the 10 eV excited energy region, several valence states arising from singly excited or doubly excited configurations are present, although they are difficult to observe from the linear ground state, either because they are symmetry-forbidden or because of their geometries (trans-bent or cis-bent). These "dark" valence states play a crucial role in the acetylene photodynamics, in such a way that the absorbing Rydberg states are more or less strongly destabilized and finally serve as doorway states toward dissociation in the VUV photolysis of this molecule.[6,28] In addition, Rydberg−valence interactions perturb to some extent the regular structure expected in the singlet Rydberg series observed in absorption.

The low-lying electronic states of acetylene have been the subject of extensive ab initio calculations in the past[22,25,29−41] which were initiated by the pioneering work of Kammer.[29,30] If one focuses on the Rydberg states, different ab initio approaches have been used for the low-lying *n*s, *n*p, and *n*d series.[22,25,26,31] Since 1984, the detailed ab initio studies by Peric et al. using large-scale MRD-CI calculations constituted a reliable reference for the experimental studies up to the $4s\sigma_g$, $3p\sigma_u$, and 3d Rydberg states,[22,33] including the characterization of the $\tilde{A}$ and $\tilde{B}$ valence states.[36] In the late 1990s Malsch et al.[25] revisited the excited structure of acetylene by means of CASPT2 calculations including both singlet and triplet manifolds in order to interpret electron energy loss spectra. More recently, Zyubin and Mebel[26] performed accurate calculations on higher Rydberg states up to $n = 11$. These authors used the OVGF Green function approach as an alternative method for excited-state calculations. They calculated the Rydberg state energies starting from the ionization limit: they subtracted the OVGF electron affinities of the positive ions from an accurate experimental value of the ionization potential (IP) and obtained in this way energies of highly excited Rydberg states within 0.05 eV from the corresponding experimental values. Nonetheless, such an approach is restricted to the prediction of vertical transition energies calculated at the linear geometry of the neutral ground state. Moreover it does not bring information on the nature of Rydberg−valence interactions as multiconfigurational methods do.

The description of Rydberg states, starting from their cation core limit, is a very old concept, extensively used by spectroscopists through the well-known Rydberg formula:

$$E(n/\lambda) = \mathrm{IP} - \frac{\mathrm{Ry}}{n^{*2}} = \mathrm{IP} - \frac{\mathrm{Ry}}{(n-\delta)^2} \qquad (1)$$

where IP is the ionization potential, n^* is the effective principal quantum number, δ is the quantum defect associated with a

† Part of the "Robert W. Field Festschrift".

* To whom correspondence should be addressed. E-mail: dolores.gauyacq@u-psud.fr (D.G.); jlievin@ulb.ac.be (J.L.).

‡ Université Libre de Bruxelles.

§ Université Paris-Sud 11.

10.1021/jp903948k CCC: $40.75
Published on Web 07/20/2009

given ℓ/λ series, and Ry is the Rydberg constant, equal to 109 735 cm^{-1} in the case of C_2H_2.[9] Many properties of the Rydberg states can be expressed via n^*-dependent scaling laws,[42,43] such as energy splittings due to the anisotropy of the core, or spatial extension of the outer $n\ell/\lambda$ Rydberg orbitals.

Fundamental concepts on molecular Rydberg states have been first introduced by Mulliken in the 1960s. Later on, an extensive experimental and theoretical work was devoted to their characterization (see for instance refs 32, 44−46). Mulliken described Rydberg molecular orbitals (MOs) in terms of hydrogenic orbitals perturbed by the inner electrons of the core.[47,48] From this description he predicted penetration effects, Rydberg−Rydberg or Rydberg−valence interactions, evolution of the Rydberg character of an orbital along a nuclear coordinate (for instance Rydbergization of a valence orbital), etc. In particular, he introduced the concept of core MO precursors for these Rydberg MOs,[47] which explains the penetrating character of a Rydberg MO (also linked to the magnitude of the quantum defect), the ℓ-mixing between Rydberg states, and the Rydberg−valence interactions.

More precisely, according to Mulliken, the external lobes of a Rydberg MO $n\ell/\lambda_{g/u}$ must mimic hydrogenic wave functions with the same $n\ell$ symmetry. Its inner part reproduces the shape of a precursor orbital, i.e., a valence MO in the ionic core, with the same symmetry $\lambda_{g/u}$, i.e., with the same angular nodal structure.[47] The precursor can be *real* or *virtual* depending whether the orbital is occupied or not in the ground state. A Rydberg MO which has a *real* precursor is expected to be penetrating, whereas a Rydberg MO with no precursor or with a *virtual* precursor is expected to be nonpenetrating.

From an ab initio approach point of view, one can ask the following question: How can a complete and accurate calculation based on a multielectron and multiconfiguration description be related to the Mulliken's concepts based on single-electron and single-configuration description? If the Rydberg state under consideration has a pure Rydberg character, one should be able to extract from the accurate ab initio calculations (energy, quantum defects, Rydberg MO shape) the same information as predicted from Mulliken's concepts. On the other hand, the departure from Mulliken's description may indicate a strong perturbation by a nearby valence state or a drastic evolution of the Rydberg MO toward valence MO. This latter kind of perturbation could in principle be analyzed in terms of mixing coefficients among calculated Rydberg and valence MOs extracted from the complete ab initio approach. These points are illustrated in this paper by a few examples on the low-lying *n*s, *n*p, and *n*d states for which comparison with experimental data can be done.

All calculations performed in this work obey the usual axis conventions and symmetries recalled in Figure 1 for the linear $D_{\infty h}$ and trans-bent C_{2h} geometries of the molecule. The electronic configurations of linear acetylene are listed in Table 1 together with the arising singlet states in both linear and trans-bent geometries. Most of the excited valence states arising from the $1\pi_u \rightarrow 1\pi_g$ excitation adopt trans-bent geometries and exhibit to different degrees a large instability toward dissociation. On the other hand, Rydberg states arising from the $1\pi_u \rightarrow n\ell/\lambda$ excitation adopt the linear equilibrium geometry of the ionic core ($D_{\infty h}$ symmetry) and are expected to be as stable as the cationic $^2\Pi_u$ ground state toward which they converge.

II. Computational Methods

All calculations were performed with the program MOLPRO[49] running on the HP-XC 4000 cluster of the ULB/VUB computing center, using the internally contracted multireference configuration interaction method (CMRCI)[50] and extended basis sets. It is particularly important[14,33] to devote special care to the choice of both the one- and *N*-electron basis sets when dealing with a mixed Rydberg−valence region, as is the case around 9 eV for acetylene. This requires the use of an extended basis set including atomic-like $n\ell$ diffuse functions suitable to represent the Rydberg orbitals of the molecular system. It also implies the definition of the active orbital spaces to be used in the complete active space self-consistent field (CASSCF)[51] and CMRCI calculations.

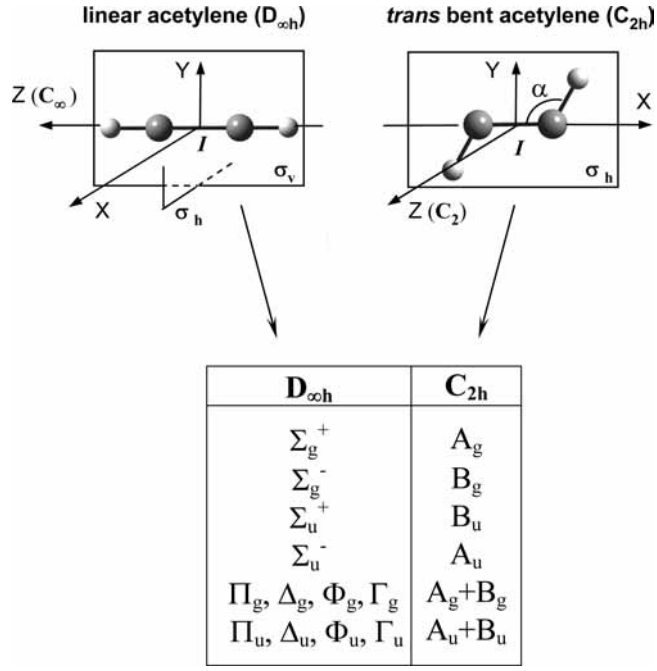

Figure 1. Molecular frame conventions and subsequent $D_{\infty h}/C_{2h}$ symmetry group correlation used for acetylene singlet states.

TABLE 1: Electronic Configurations in Linear Geometry and Related Singlet Electronic States of Acetylene ($D_{\infty h}$ and C_{2h} Symmetry)[a]

electronic configuration $D_{\infty h}$[b]	type	electronic state	
		$D_{\infty h}$	C_{2h}
[core] $(1\pi_u)^4$	GS (g)	$^1\Sigma_g^+$	^1A_g
... $(1\pi_u)^3$ $(1\pi_g)^1$	$V^{(SE)}$ (u)	$^1\Sigma_u^+$, $^1\Sigma_u^-$, $^1\Delta_u$	^1B_u (2), ^1A_u (2)
... $(1\pi_u)^2$ $(1\pi_g)^2$	$V^{(DE)}$ (g)	$^1\Sigma_g^+$ (3), $^1\Sigma_g^-$, $^1\Delta_g$ (2), $^1\Gamma_g$	^1A_g (6), ^1B_g (4)
... $(1\pi_u)^3$ $(ns\sigma_g)^1$	R (u)	$^1\Pi_u$	^1A_u, ^1B_u
... $(1\pi_u)^3$ $(np\sigma_u)^1$	R (g)	$^1\Pi_g$	^1A_g, ^1B_g
... $(1\pi_u)^3$ $(np\pi_u)^1$	R (g)	$^1\Sigma_g^+$, $^1\Sigma_g^-$, $^1\Delta_g$	^1A_g (2), ^1B_g (2)
... $(1\pi_u)^3$ $(nd\sigma_g)^1$	R (u)	$^1\Pi_u$	^1A_u, ^1B_u
... $(1\pi_u)^3$ $(nd\pi_g)^1$	R (u)	$^1\Sigma_u^+$, $^1\Sigma_u^-$, $^1\Delta_u$	^1A_u (2), ^1B_u (2)
... $(1\pi_u)^3$ $(nd\delta_g)^1$	R (u)	$^1\Pi_u$, $^1\Phi_u$	^1A_u (2), ^1B_u (2)

[a] GS stands for ground state, $V^{(SE)}$ for singly excited valence state, $V^{(DE)}$ for doubly-excited valence state, R for Rydberg state. The number of electronic states arising from a specific configuration is indicated in parentheses when more than one. [b] All configurations include the core configuration [core] $\equiv [(1\sigma_g)^2(1\sigma_u)^2(2\sigma_g)^2(2\sigma_u)^2(3\sigma_g)^2]$.

II.A. Valence and Rydberg Orbital Basis Sets. The correlation-consistent and polarized triple-ζ (cc-pVTZ) basis set of Dunning[52] is used for describing the valence electronic structure of the molecule. It is supplemented by diffuse Gaussian *s*, *p*, and *d* atomic functions aiming to represent the Rydberg $n\ell/\lambda$ molecular orbitals. These functions are placed[22,25] on a dummy atom centered in the middle of the C−C bond. The

few Rydberg basis sets tabulated in the literature are either limited to a small number of Gaussian primitives (2, 1, and 1 for *s*, *p*, and *d*, respectively[53]) or on the contrary are containing a too large number (up to 10 per *l* value for describing the Rydberg series up to $n = 11$). In this work we decided to optimize *s*, *p*, and *d* Rydberg basis sets answering to our needs. Being interested in the $n = 3-5$ series, we have optimized even-tempered basis sets built on a reasonable number *k* of primitives ($5 \leq k \leq 7$) for getting the desired flexibility. The parameters τ and ν defining the geometric progression of the Gaussian exponents $\alpha_i = \tau\nu^i$ ($i = 1$ to *k*) were optimized by numerical minimization of the state-averaged CASSCF energies of the molecular states of acetylene arising from the $n\,/\,\lambda$ ($/ = 0$, 1, and 2) of interest. The optimized parameters are

$$n\text{s}\ (n = 3-4): \quad k = 5, \quad \tau = 0.02, \quad \nu = 5$$
$$n\text{p}\ (n = 3-4): \quad k = 5, \quad \tau = 0.01, \quad \nu = 2.2$$
$$n\text{p}\ (n = 3-5): \quad k = 7, \quad \tau = 0.005, \quad \nu = 3$$
$$n\text{d}\ (n = 3-4): \quad k = 5, \quad \tau = 0.05, \quad \nu = 2.5$$

These results exhibit the expected dependence of the parameter values with $/$and with the maximum *n* value. Test calculations demonstrated the pertinence of these parameters for all states of a given $n/$series.

Two different basis sets, referred to below as VTZ+sd and VTZ+p, were used for calculating the gerade (g) and ungerade (u) states, respectively, for centrosymmetric geometries.

These basis sets are formed by the cc-pVTZ valence set augmented by the (*n*s + *n*d) and *n*p Rydberg basis sets, respectively. Note that the Rydberg basis sets were left uncontracted in all calculations, providing the required flexibility to the calculated wave functions.

II.B. Active Spaces and Computational Strategy. Our computational strategy is based on the definition of the active orbital spaces and on the state average CASSCF optimization schemes adopted for calculating the different type of states reported in Table 1 with the following abbreviations: GS (ground state), $V^{(SE)}$ (singly excited valence state), $V^{(DE)}$ (doubly excited valence state), $R^{(g)}$ and $R^{(u)}$ (Rydberg states). The full MO space subtending these states can be split accordingly into the following:

(i) the valence space V (GS + $V^{(SE)}$ + $V^{(DE)}$), {$1\sigma_g$, $1\sigma_u$, $2\sigma_g$, $2\sigma_u$, $3\sigma_g$, $1\pi_u$, $1\pi_g$};
(ii) the Rydberg $R^{(u)}$ space, {$3s\sigma_g$, $4s\sigma_g$} U {$3d\sigma_g$, $3d\pi_g$, $3d\delta_g$};
(iii) the Rydberg $R^{(g)}$ space, {$3p\sigma_u$, $3p\pi_u$, $4p\sigma_u$, $4p\pi_u$, $5p\sigma_u$, $5p\pi_u$}.

The V + $R^{(g)}$ or V + $R^{(u)}$ orbital spaces were used for calculating the u and g electronic states, respectively, adopting accordingly the VTZ+p or VTZ+sd basis sets. Let us point out the importance of the $1\pi_g$ MO that contributes to the excited valence states ($V^{(SE)}$ and $V^{(DE)}$) interacting with some of the Rydberg states of interest. The CASSCF active spaces are built from the full g or u orbital spaces, keeping closed all valence σ orbitals. This restriction is released at the CMRCI level, where a frozen core of four electrons occupying the $1\sigma_g$ and $1\sigma_u$ MOs is maintained, while the remaining 10 electrons are explicitly correlated.

State average (SA) CASSCF calculations have been performed for optimizing a common active space of MOs for all states arising from a given Rydberg series or from a Rydberg complex. Valence states energetically located below or within these series were also included in the SA procedure. Let us point out that MOLPRO calculations exploit the symmetry of the D_{2h} abelian subgroup and that the twofold degeneracy of the $\Lambda \neq 0$ states is guaranteed by the SA procedure.

Applying the above prescriptions to the u states implies an SA of the following 22 D_{2h} states: ^1A_g, {$^1B_{2u}$, $^1B_{3u}$}(5), {$^1B_{1u}$, ^1A_u}(5), ^1A_u, corresponding in $D_{\infty h}$ symmetry to the following 14 eigenstates: $^1\Sigma_g^+$ (GS), $^1\Delta_u$, and $^1\Sigma_u^-$ ($V^{(SE)}$) states, $^1\Pi_u$ (2) ($R^{(u)}$ 3s and 4s), $^1\Pi_u$ ($R^{(g)}$ $3d\sigma_g$), $^1\Pi_u$ and $^1\Phi_u$ ($R^{(u)}$ $3d\delta_g$), $^1\Delta_u$ (2), $^1\Sigma_u^-$ (2), and $^1\Sigma_u^+$ (2) ($R^{(u)}$ $3d\pi_g$ and $4d\pi_g$). The number of states is given in parentheses, if larger than 1, and the curly brackets indicate pairs of degenerated electronic components.

The number of SA g states amounts to 19 in D_{2h} symmetry: ^1A_g (4), {^1A_g, $^1B_{1g}$}(3), $^1B_{1g}$ (3), {$^1B_{2g}$, $^1B_{3g}$}(3), leading in $D_{\infty h}$ symmetry to the following 13 eigenstates: $^1\Sigma_g^+$ (GS), $^1\Sigma_g^+$ (3) ($R^{(g)}$ $np\sigma_u$, $n = 3-5$), $^1\Sigma_g^-$ (3), $^1\Pi_g$ (3), and $^1\Delta_g$ (3) ($R^{(g)}$ $np\pi_u$, $n = 3-5$).

Let us point out that the GS has been included in the $R^{(u)}$ space although being of g symmetry in order to provide a consistent reference for the term energy calculations. Also note the addition of $4d\pi_g$ into the $R^{(u)}$ space because of the significant effect observed on the stabilization of the $3d\pi_g$ arising states.

II.C. Calculation of Molecular Properties. All calculated properties reported in the next sections have been obtained at CMRCI level of theory. All reported energies, to be referred to below as CMRCI+Q, include the Davidson correction for unlinked quadruple excitations.[54] The size of the configuration interaction (CI) matrices range from 10^6 to 2.2×10^6 contracted configuration state functions (CSF), depending on the considered spatial symmetry and the number of states to be converged in the matrix diagonalization. Geometry optimizations were performed for all states at CMRCI+Q level using a quadratic steepest descent algorithm. Such calculations being demanding in computer time, we have restricted the occupation of the Rydberg MOs to 0 or 1 electron in the MRCI wave function, resulting in a reduction of the computer time by a factor of up to 10 without significant loss of accuracy in the calculated energies (<0.01 eV). All CMRCI+Q term energies were, however, recalculated at the equilibrium geometries without these restrictions. Natural CMRCI orbitals are used for visualizing the features of the Rydberg orbitals, drawn with the MOLDEN program.[55]

III. Results and Discussion

III.A. Landscape of the Excited Singlet States of Acetylene. ***III.A.1. Summary of the Earlier Experimental and Theoretical Investigations.*** A comprehensive review of the excited singlet electronic states of C_2H_2 up to 1999 has been presented by Peric and Peyrimhoff,[33] including experimental and theoretical investigations. A short updated summary is given below.

Among the observed Rydberg states, several components from $n = 3$ to $n = 10$ for the $^1\Sigma_u^+$ and $^1\Pi_u$ symmetries[8] have been observed in absorption. The analysis of these $n/$series has been extended thanks to resonantly enhanced multiphoton ionization (REMPI) spectroscopy: new components of the 3d complex, namely, $^1\Delta_u$ ($\tilde{H}'$ $3d\pi_g$) and $^1\Phi_u$ ($\tilde{F}'$ $3d\delta_g$), have been observed by (3 + 1) photon REMPI.[11,56] Three-photon excitation also allowed us to complement the analysis of the *n*s and *n*d series up to $n = 10$ (ref 10). In addition, the *n*p states up to $n = 6$ have been characterized for the first time by two-color REMPI spectroscopy. Among the *n*p Rydberg states, only the $^1\Sigma_g^+$ and the $^1\Delta_g$ components have been observed.[9,57,58] Finally higher-lying *n*f states have been observed by two-color REMPI spectroscopy[12] ($n = 18-35$).

TABLE 2: Geometry (Distances in angstroms, Angles in deg), Main Orbital Excitation, and Term Energies (in eV) of the Acetylene Electronic States

			CMRCI+Q calculations[a] (this work, otherwise indicated)			vertical energies				
type	label	main orbital excitation	$R_{CC}/R_{CH}/\alpha$	adiabatic T_e	exptl T_0	CMRCI+Q this work	MRD-CI ref 33	OVGF/CCSD[b]	CASSCF[c]	CASPT2[c]
GS	$\tilde{X}\ ^1\Sigma_g^+$		1.210/1.065/180.0	0	0		0	0	0	0
V	$\tilde{A}\ ^1A_u$	$1\pi_g$	1.380/1.097/121.7[d]	5.24[d] (5.26)[d]	5.23[e]					(5.19)
V	$\tilde{B}\ ^1B_u$	$1\pi_g$	1.337/1.077/148.5[d]	6.78[d] (6.78)[d]	6.71[f]					(6.68)
V	$2\ ^1A_u$	$1\pi_g$	1.327/1.065/171.5[d]	6.91[d] (6.90)[d]	7.2[g]					(6.83)
V	$\tilde{C}'\ ^1A_g$	$(1\pi_g)^2$	1.621/1.096/104.5[h]	7.53	7.72[i]					
R	$\tilde{C}\ ^1\Pi_u$	$3s\sigma_g$	1.254/1.073/180.0[d]	8.174	8.16[j]	8.250	8.0	8.165/8.386	8.30	
R	$3p\ ^1\Pi_g$	$3p\sigma_u$	1.266/1.112/180.0	8.433		8.669	8.4	8.623/8.781	8.60	
R	$3p\ ^1\Delta_g$	$3p\pi_u$	1.252/1.077/180.0	8.998	9.01[k]	9.080	8.9	9.066/9.218	8.96	
R	$3p\ ^1\Sigma_g^-$	$3p\pi_u$	1.252/1.078/180.0	9.055		9.158	8.9	9.072/9.274	8.92	
R	$3p\ ^1\Sigma_g^+$	$3p\pi_u$	1.252/1.079/180.0	9.157	9.21[k]	9.242	9.0	−/9.429	9.06	
R	$\tilde{D}\ ^1\Pi_u$	$3d\sigma_g$	1.254/1.113/180.0[d]	9.374	9.24[j]	9.517	9.4	9.427/9.601	9.55	
V	$\tilde{E}\ ^1B_u$	$1\pi_g$	1.276/1.102/161.2[d]	9.36 (9.39)	9.25[l]				10.65	
R	$\tilde{F}\ ^1\Sigma_u^+$	$3d\pi_g$	1.262/1.081/180.0	9.532	9.27[j]	9.649	9.4	−/9.768	9.65	
R	$\tilde{F}'\ ^1\Phi_u$	$3d\delta_g$	1.254/1.078/180.0	9.886	9.91[m]	9.974	9.8	9.947/10.139	9.93	
R	$\tilde{H}\ ^1\Pi_u$	$3d\delta_g$	1.254/1.078/180.0	9.903	9.98[j]	9.991	9.8	9.948/10.160	9.93	
R	$\tilde{G}\ ^1\Pi_u$	$4s\sigma_g$	1.254/1.078/180.0	9.922	9.93[j]	10.016	9.7	9.982/10.190		
R	$\tilde{H}'\ ^1\Delta_u$	$3d\pi_g$	1.259/1.080/180.0	9.975	10.0[n]	10.084	9.8	10.018/10.232	9.73−9.88	
R	$^1\Sigma_u^-$	$3d\pi_g$	1.259/1.079/180.0	9.974		10.083	9.8	9.919/10.229	9.81	
R	$4p\ ^1\Pi_g$	$4p\sigma_u$	1.262/1.095/180.0	10.014		10.169		10.116/10.295		
R	$4p\ ^1\Delta_g$	$4p\pi_u$	1.254/1.077/180.0	10.175	10.24[k,o]	10.268		10.259/10.447		
R	$4p\ ^1\Sigma_g^-$	$4p\pi_u$	1.254/1.077/180.0	10.193		10.286		10.260/10.463		
R	$4p\ ^1\Sigma_g^+$	$4p\pi_u$	1.255/1.078/180.0	10.227	10.29[o]	10.321		−/10.515		
R	$5p\ ^1\Pi_g$	$5p\sigma_u$	1.254/1.080/180.0	10.613		10.719		10.656/10.847		
R	$5p\ ^1\Delta_g$	$5p\pi_u$	1.253/1.075/180.0	10.667	10.71[o]	10.761		10.739/10.935		
R	$5p\ ^1\Sigma_g^-$	$5p\pi_u$	1.253/1.075/180.0	10.674		10.768		10.739/10.940		
R	$5p\ ^1\Sigma_g^+$	$5p\pi_u$	1.255/1.075/180.0	10.687	10.73[o]	10.783		−/10.960		
cation	$\tilde{X}\ ^2\Pi_u$		1.247/1.075/180.0[p]	11.38[p]	10.401[q]					

[a] All calculations are performed at the VTZ+Ryd/CMRCI level of theory. T_e values in parentheses are calculated with an AVQZ basis set at VTZ optimized geometries. [b] From Zyubin and Mebel (ref 26). The two levels of theory are using different basis sets. [c] From Malsch et al. (ref 25). Values in parentheses correspond to optimized CASSCF geometries. [d] From Blanchet et al. (ref 14). [e] From Ingold and King (ref 59). [f] From Foo and Innes (ref 60). [g] From Dressler and Allan (ref 75). [h] From Liévin (ref 23). [i] From Lundberg et al. (ref 62). [j] From Herman and Colin (ref 8). [k] From Ashfold et al. (ref 9). [l] From Herman and Colin (ref 7). [m] From Ashfold et al. (ref 56). [n] From Fillion et al. (ref 11). [o] From Tsuji et al. (ref 58). [p] From Boyé-Péronne et al. (ref 76). [q] From Ruppert and Merkt (ref 77).

Among the valence states, the trans-bent $\tilde{A}\ ^1A_u$ state has been first observed by Ingold and King.[59] Later on, the $\tilde{B}\ ^1B_u$ state has been characterized[60] and correlated with the $^1\Delta_u$ symmetry of the same $(1\pi_u)^3(1\pi_g)^1$ linear configuration as the $\tilde{A}$ state (see Table 1). The spectra of these two states have been theoretically interpreted by Peric et al.[36] A third state arising from the same configuration, the $\tilde{E}\ ^1B_u$ state correlating with the $^1\Sigma_u^+$ linear symmetry, has been first assigned by Herman and Colin.[7] This assignment has been unambiguously confirmed both experimentally and theoretically, by photoelectron spectroscopy associated with REMPI (REMPI-PES), and by ab initio calculations.[14] Note that another assignment of the $\tilde{E}$ state was earlier proposed from double-resonance spectroscopy by Lundberg et al.[61] as a nonplanar cis-bent state, but this assignment was revised[14] and rather associated to a member of the 3p series following the analysis of Takahashi et al.[57]

The $\tilde{C}'\ ^1A_g$ state arising from the $(1\pi_u)^2(1\pi_g)^2$ configuration adopts a strongly bent equilibrium geometry. This state was discovered experimentally by Robert Field's group via two-color experiments[62] and is the only doubly excited valence state characterized both experimentally and theoretically[23] up to now.

III.A.2. Present Calculations: Energetics and Geometrical Considerations. Table 2 summarizes the optimized calculated geometries and energies for the lowest singlet states of acetylene including valence states and *n*s, *n*p, and *n*d Rydberg states lying in the same energy range, presented with increasing energy.

A significant increase from the ground-state geometry affects the CC bond length in all valence states of Table 2, which is well-known for all unsaturated hydrocarbons excited into the π^* orbital. More quantitatively, this lengthening amounts to +0.12 Å for R_{CC} upon single excitation to the $1\pi_g$ antibonding orbital (in good agreement with ref 36) and to +0.41 Å in the doubly excited $\tilde{C}'$ state. This indicates again the crucial role played by this antibonding $1\pi_g$ orbital in the stability of excited acetylene.

The level of accuracy of our theoretical calculations can be tested through the comparison between calculated and experimental energies when available, as shown in Table 2. Most of the calculated adiabatic energies lie within less than 0.1 eV from the experimental ones. Moreover, the level pattern within the 4s + 3d Rydberg supercomplex is in perfect agreement with the observed levels, albeit with a slight global shift.[11]

Table 2 also reports vertical energies calculated in this work to compare with ab initio calculations performed by Peric et al.[22] and by Zyubin and Mebel.[26] In the energy range shown in Table 2 (below 11 eV) our calculations complete those of ref 22 up to 5p and include the $\tilde{E}$ valence state. They are also in good agreement with the values of ref 26. The method used by Zyubin and Mebel allows us to extend the calculations up to higher *n* states and to deal with *n*f Rydberg states, whereas ab initio approaches as the one presented here become inappropriate due to the rapidly increasing size of the basis sets.

III.A.3. Rydberg Character of the Excited States of Acetylene Derived from the Present ab Initio Calculations. The calculated effective principal quantum numbers and quantum defects for the low-lying Rydberg states calculated in this

TABLE 3: Calculated Properties Indicating the Rydberg Character of Acetylene: $\langle R^2 \rangle$ Spatial Extent (in a_0^2), n^* Effective Principal Quantum Number, and δ Quantum Defect for the Rydberg States and Comparison with Experiment

	state	main orbital excitation	$\langle R^2 \rangle^a$	$n^*_{\text{calcd}}{}^b$	$n^*_{\text{exptl}}{}^c$	$\delta_{\text{calcd}}{}^b$	$\delta_{\text{exptl}}{}^c$
GS	$\tilde{X}^1\,\Sigma_g^+$		25.3				
V	$1\,^1\Sigma_u^-$	$1\pi_g$	30.5				
V	$1\,^1\Delta_u$	$1\pi_g$	32.2				
R	$\tilde{C}\,^1\Pi_u$	$3s\sigma_g$	68.7	2.05	2.05	0.95	0.95
R	$3p\,^1\Pi_g$	$3p\sigma_u$	78.5	2.14		0.86	
R	$3p\,^1\Delta_g$	$3p\pi_u$	93.3	2.38	2.38	0.62	0.62
R	$3p\,^1\Sigma_g^-$	$3p\pi_u$	95.5	2.41		0.59	
R	$3p\,^1\Sigma_g^+$	$3p\pi_u$	109.2	2.46	2.49	0.54	0.51
R	$\tilde{D}\,^1\Pi_u$	$3d\sigma_g$	108.3	2.59	2.51	0.41	0.49
V	$\tilde{E}\,^1B_u$	$1\pi_g$ ($4a_g$, $1b_g$)	30.1				
R	$\tilde{F}\,^1\Sigma_u^+$	$3d\pi_g$	111.8	2.69	2.53	0.31	0.47
R	$\tilde{F}'\,^1\Phi_u$	$3d\delta_g$	156.2	2.99	3.02	0.01	−0.02
R	$\tilde{H}\,^1\Pi_u$	$3d\delta_g$	163.7	3.01	3.09	−0.01	−0.09
R	$\tilde{G}\,^1\Pi_u$	$4s\sigma_g$	268.1	3.03	3.04	0.97	0.96
R	$\tilde{H}'\,^1\Delta_u$	$3d\pi_g$	200.2	3.08	3.12	−0.08	−0.12
R	$^1\Sigma_u^-$	$3d\pi_g$	195.2	3.08		−0.08	
R	$4p\,^1\Pi_g$	$4p\sigma_u$	312.8	3.13		0.87	
R	$4p\,^1\Delta_g$	$4p\pi_u$	356.4	3.32	3.42	0.68	0.58
R	$4p\,^1\Sigma_g^-$	$4p\pi_u$	361.6	3.35		0.65	
R	$4p\,^1\Sigma_g^+$	$4p\pi_u$	393.4	3.40	3.50	0.60	0.50
R	$5p\,^1\Pi_g$	$5p\sigma_u$	1017.8	4.14		0.86	
R	$5p\,^1\Delta_g$	$5p\pi_u$	1047.9	4.29	4.44	0.71	0.56
R	$5p\,^1\Sigma_g^-$	$5p\pi_u$	1042.8	4.31		0.69	
R	$5p\,^1\Sigma_g^+$	$5p\pi_u$	1002.3	4.35	4.50	0.65	0.50

[a] Computed at the cation ground-state geometry except for the $\tilde{E}$ state for which it was calculated at the trans-bent equilibrium geometry given in ref 14. [b] Derived from the calculated values of Table 2 by using the adiabatic term energy and the value 11.407 eV for the IP, taken from ref 76. [c] Derived from the experimental values reported in Table 2 and from the IP value of 11.401 eV from ref 77.

TABLE 4: Precursor Valence Orbitals and Rydberg Molecular Orbitals (MO) of Acetylene

G.S. configuration	$[(1\sigma_g)^2(1\sigma_u)^2]$	$(2\sigma_g)^2(2\sigma_u)^2(3\sigma_g)^2(1\pi_u)^4(1\pi_g)^0$			
MO precursor	$(2\sigma_g)$	$(2\sigma_u)$	$(3\sigma_g)$	$(1\pi_u)$	$(1\pi_g)$
Rydberg MO/ State	$ns\sigma_g\,^1\Pi_u$	$np\sigma_u\,^1\Pi_g$	$nd\sigma_g\,^1\Pi_u$	$np\pi_u\,^1\Delta_g$ $np\pi_u\,^1\Sigma_g^-$ $np\pi_u\,^1\Sigma_g^+$	$nd\pi_g\,^1\Delta_u$ $nd\pi_g\,^1\Sigma_u^-$ $nd\pi_g\,^1\Sigma_u^+$

work are reported in Table 3 and show a good agreement with corresponding experimental values. In addition Table 3 presents the averaged spatial extent $\langle R^2 \rangle$ for the Rydberg and valence states under consideration in this paper. This calculated quantity brings valuable information on the Rydberg character of the state. The valence states exhibit an $\langle R^2 \rangle$ value less than 35 au, whereas Rydberg states have much larger spatial extent increasing roughly as n^{*4}, as shown on the example of the 3p, 4p, and 5p states.

III.A.4. Calculated Outer Molecular Orbitals and Their Relation to Mulliken's Concepts. Table 4 summarizes the valence MOs of ground-state acetylene, which serve as precursors for the low-lying *n*s, *n*p, and *n*d Rydberg MOs of acetylene following the prescriptions of Mulliken's paper.[47] The lowest four valence MOs of the core are occupied in the ground state. Therefore it can be predicted from Table 4 that $ns\sigma_g$, $np\sigma_u$, $nd\sigma_g$, and $np\pi_u$ Rydberg MOs are penetrating. On the other hand, the $nd\pi_g$ Rydberg MOs with their virtual $1\pi_g$ MO, as well as the $nd\delta_g$ Rydberg MOs, with no precursor at all, should be nonpenetrating. The ab initio calculations performed in the present work allow us to extract the shape of the outer MO of the Rydberg states and to compare these shapes with the predictions of Table 4. This is done in details in the following sections III.B and III.C for the lowest *n*p and *n*s−*n*d complexes.

III.B. Low-Lying Members of the Gerade *n*p Rydberg Series. ***III.B.1. np Rydberg Molecular Orbitals and Their Precursors.*** Isocontours plots of the $np\sigma_u$ and $np\pi_u$ Rydberg orbitals calculated at the cation ground-state geometry are displayed in Figure 2 for the different electronic components of the 3p, 4p, and 5p complexes. These pictures are obtained from the natural orbitals of the MRCI wave functions corresponding to the considered Rydberg states. The isocontour plots of Figure 2 are shown at the same scale, and each of them is accompanied with an inset presenting a zoom of the inner part of the MO. All insets are drawn at the same scale again, as indicated by the size of the nuclear skeleton.

The external lobes of these orbitals are quasi-hydrogenic as expected for pure Rydberg orbitals. Furthermore they nicely follow an n^{*2} radial extension law.

Attention can be drawn on the shape of the inner part of these Rydberg MOs displayed in the insets of Figure 2. Following Jungen,[63] the shape of a Rydberg orbital Φ_R can be approximated by

$$\Phi_R = (1 - S^2)^{-1/2}(\Phi_{Hyd} - S\Phi_V) \qquad (2)$$

taking into account the orthogonality between the hydrogenic atomic orbital Φ_{Hyd} corresponding to the *n*/ state associated

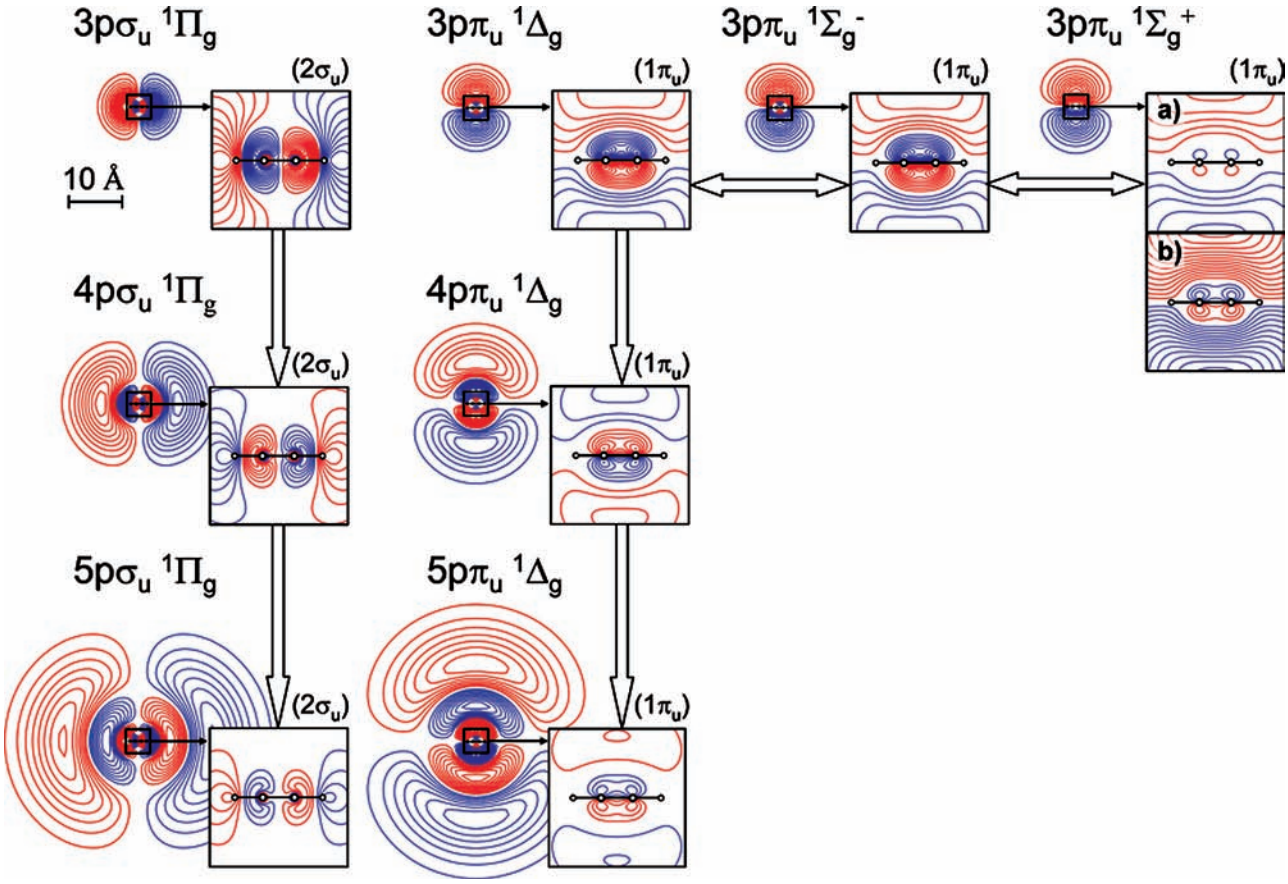

Figure 2. Isocontour maps of the *n*p Rydberg molecular orbitals of acetylene ($n = 3-5$), calculated at the cation ground-state geometry from CMRCI natural orbitals. Blue (red) line refers to the negative (positive) value of the wave function. The length scale used for all plots is highlighted by a 10 Å tick mark on the top left of the figure. All insets are drawn at the same scale indicated by the size of the nuclear skeleton. Orbital isocontour step values adopted in the drawings are 0.0025, 0.00125, and 0.0005 for 3p, 4p, and 5p, respectively, and 0.005 for all insets, except for inset b of the 3p $^1\Sigma_g^+$ state for which a lower value of 0.001 is used. Outermost contours of MOs correspond to the step value.

with the Rydberg orbital and its valence precursor MO Φ_V. The positive value of the overlap integral S between Φ_V and Φ_{Hyd} and the minus sign in eq 2 gives rise to a radial node surrounding the inner part of the orbitals. As observed in Figure 2, this node separates the signature of the core precursor from the external lobes of the hydrogenic atomic-like orbital.

For the *n*p Rydberg states, two real precursors are considered, namely, the $2\sigma_u$ orbital for the $np\sigma_u$ Rydberg MOs and the $1\pi_u$ orbital for the $np\pi_u$ Rydberg MOs. As shown in the insets of Figure 2, the $np\sigma_u$ orbitals exhibit an inner shape almost identical to the $2\sigma_u$ core valence orbital, whereas the $np\pi_u$ orbitals exhibit an inner shape very close to the $1\pi_u$ core valence orbital, except for the $np\pi_u$ $^1\Sigma_g^+$ state which is examined below. The presence of these real precursors explains the penetrating character of the *n*p states and their large quantum defects (see Table 3). In addition the inner function shows a decreasing amplitude with n, as expected from the $(1/n^*)^{3/2}$ scaling law.

Another comment is worth noting in Figure 2: as stated by Mulliken,[47] a Rydberg MO and its precursor present the same angular nodal structure. This is the case for all *n*p MOs having a precursor. In addition, because of the orthogonality requirement reported above, the number of radial nodes n_r of the lowest 3p Rydberg orbital is incremented by one unit from its precursor, by two for the 4p MO, by three for the 5p MO, and so on. This rule can be checked in Figure 2.

The $1\pi_u$ core MO can in principle serve as a real precursor for the $^1\Delta_g$, $^1\Sigma_g^-$, and $^1\Sigma_g^+$ states involving the $np\pi_u$ Rydberg MOs, as shown in Figure 2, but it clearly happens that the $^1\Sigma_g^+$ state exhibits a less pronounced signature of the precursor than the two other states (Note that the same situation holds for $n = 4$ and 5.) The $^1\Sigma_g^+$ state can therefore be considered as less penetrating than the $^1\Delta_g$ and $^1\Sigma_g^-$ states and should have a smaller quantum defect value. Disappointingly, the difference is not so large (see Table 3). The quantum defect is, however, derived from purely energetic considerations and, therefore, takes into account all possible perturbations from the hydrogenic model. This includes, in addition to penetrating effects, external perturbations such as Rydberg−valence interactions, as discussed in section III.B.3 below. A similar effect was earlier noticed by Mulliken in the case of the $3p\pi_u$ $^1\Sigma_g^+$ state of the isoelectronic N_2 molecule.[48]

III.B.2. Scaling Laws and Core Anisotropy in the np Complexes. The *n*p Rydberg states are penetrating states and exhibit typical quantum defect values between 0.5 and 0.7. As shown in Table 3, a fair agreement is obtained between theory and experiment for the 3p and 4p states. The agreement for the 5p complex is not as good and shows the limitation reached by the present ab initio approach for describing states with large diffuse orbitals.

The acetylene *n*p Rydberg complexes present a very good example for evaluating the core anisotropy and the symmetry splitting due to a noncentral molecular symmetry. The $\sigma-\pi$ anisotropy induced by the intramolecular axial field is measured by the ΔE energy splitting between the pσ component and the weighted-average energy of the pπ components. An additional energy splitting δE smaller than ΔE arises from a coupling

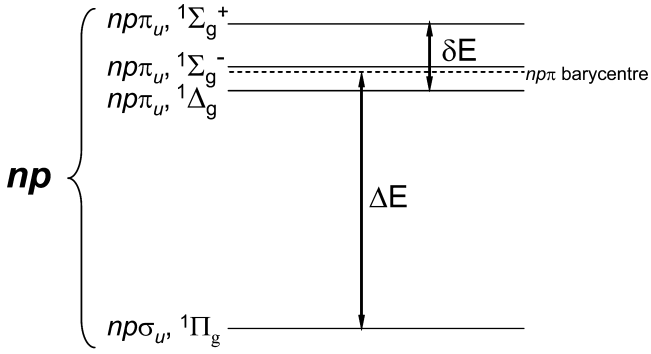

n	ΔE (eV)	$n^{*3}\times\Delta E$	δE_{exp} (eV)	δE (eV)	$n^{*3}\times\delta E$
3	0.619	7.6	0.20	0.159	2.0
4	0.179	6.5	0.05	0.052	1.9
5	0.061	4.9	0.02	0.020	1.6

Figure 3. Illustration of the core anisotropy in the *n*p Rydberg complexes of acetylene. ΔE is the energy difference between the $np\sigma$ component and the barycenter of the $np\pi$ components. The quantum defects of the table are derived from the energy calculated in this work and the ionization potential calculated in ref 76 (i.e., 11.407 eV).

between the $np\pi$ orbitals with the open-shell core orbitals. These splittings are schematically depicted in Figure 3. Ab initio approaches such as the present one are expected to precisely account for such anisotropy, which originates from a pure electrostatic interaction with the internal core molecular field. It is interesting to see how they are able to predict scaling laws with respect to n^*.

With increasing principal quantum number n, the penetration effect decreases in such a way that the ΔE and δE energy splittings follow a $1/n^{*3}$ scaling law for a pure Rydberg character. The table of Figure 3 illustrates the results found for the $n = 3$, 4, and 5 *n*p Rydberg states. Again, a slightly lower agreement is found on what concerns the 5p complex.

Comparison with the experimental data can be carried out only for the δE splitting due to the lack of observation of predissociated members of the *n*p complex.[57] The observed δE values match very well the calculated ones, as shown in the table of Figure 3.

III.B.3. Rydberg−Valence Interactions in the np Complexes. Experimentally, some of the low-lying *n*p ($n = 3$ and 4) Rydberg states of acetylene undergo rapid predissociation and could not be observed via two-color REMPI experiments[57,58] except for a recent mass analysis of resulting fragments.[64] Predissociation most probably occurs via a route through avoided crossings and conical intersections between excited Rydberg potential energy surfaces (PES) and unstable bent valence states. This section presents a typical example of such an interaction between the doubly excited valence $\tilde{C}'$ state and the 3p, 4p, and 5p Rydberg states. This interaction is illustrated in Figure 4 by a cut in the CASSCF PES of trans-bent acetylene. The potential curves of ^1A_g and ^1B_g species are presented in two different panels linked by the common linear geometry. The reaction coordinate used in these calculations corresponds to a route through the PES, smoothly connecting the equilibrium geometry of the $\tilde{C}'$ state[23] ($\alpha = 104.5°$, $R_{CC} = 1.621$ Å, and $R_{CH} = 1.096$ Å) to the linear geometry of the neutral ground state ($R_{CC} = 1.22$ Å and $R_{CH} = 1.06$ Å). The active coordinate is the trans-bending angle α (see Figure 1), which has been chosen as abscissa of the graphs. The 2 ^1A_g and 1 ^1B_g states correlate diabatically at linear geometry with the $^1\Sigma_g^+$ and $^1\Gamma_g$ states, respectively. Both states, lying above the ionization limit

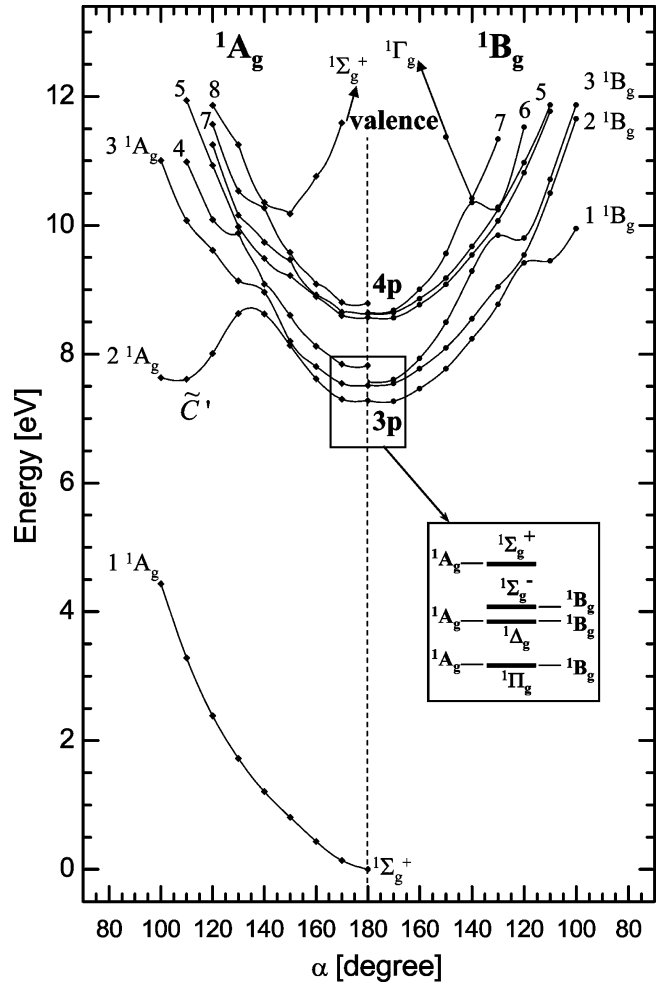

Figure 4. Cuts in the ^1A_g and ^1B_g potential energy surfaces for the ground state, 3p, and 4p Rydberg states of acetylene along a C_{2h} trans-bending path (see text for the definition of the coordinates). These results are obtained at the CASSCF state-averaged level of theory including eight ^1A_g states and seven ^1B_g states.

at linear geometry, arise from the doubly excited $(1\pi_u)^2$ $(1\pi_g)^2$ configuration. Their spectacular stabilization along the bending coordinate, predicted by the Walsh correlation diagram,[65] induces a crossing of the whole *n*p series in a cascade of avoided crossings. From the stronger bent character of the $4a_g$ orbital than the $1b_g$ one, it results that the 2 ^1A_g state, labeled $\tilde{C}'$, stabilizes more than its ^1B_g counterpart and exhibits a minimum stationary point on its PES, characterized both experimentally[62] and theoretically.[23]

The Rydberg−valence mixing highlighted in Figure 4 is responsible for perturbations in the *n*p series. It mainly contributes to the departure from the pure hydrogenic Rydberg behavior, as already pointed out before in the case of the 3p $^1\Sigma_g^+$ state. Though the description of the decay of the states along a dissociation coordinate is out of the scope of the present paper, one can predict the opening of predissociation routes along the trans-bending path described above, through conical intersections resulting from the crossing of the states of gerade symmetry represented in Figure 4 with ungerade states.

Rydberg−valence interactions are in principle well-described by ab initio calculations as was earlier shown for instance by Buenker and Peyerimhoff[66] on other molecules.

III.C. Ungerade *n*s−*n*d Rydberg Series ($n = 3$−4). Observation of the *n*s−*n*d Rydberg manifold for $n = 3$ and 4 has been done by one-photon or three-photon excitation in the 8−10

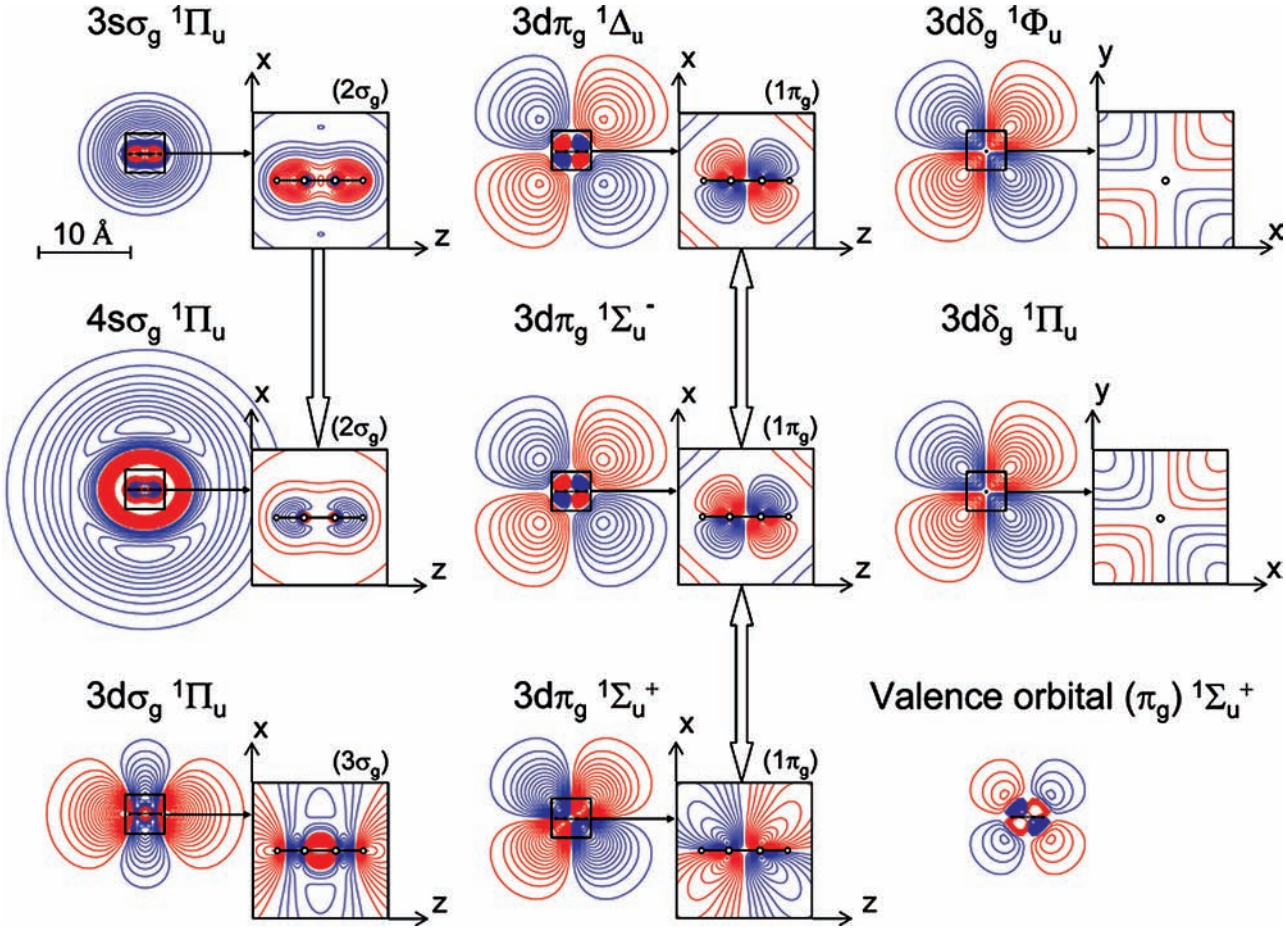

Figure 5. *n*s−*n*d Rydberg molecular orbitals of acetylene from MRCI natural orbitals. Blue (red) line refers to the negative (positive) value of the wave function. Note that the 3dδ_g MOs are shown in a plane perpendicular to the molecular axis and that the $^1\Sigma_u^+$ state arising from 3dπ_g is described by two MOs illustrating the Rydberg−valence mixing (see text). Isocontour step values are 0.002 and 0.0005 for $n = 3$ and 4, respectively, and 0.005 for all insets.

eV energy range.[7,8,10,11,14,56] At low energy, the $\tilde{C}$ 3sσ_g $^1\Pi_u$ state exhibits a very broad and diffuse absorption structure around 8.16 eV.[8,28] At intermediate energy between 9.24 and 9.27 eV, the $\tilde{D}$ 3dσ_g $^1\Pi_u$ and $\tilde{F}$ 3dπ_g $^1\Sigma_u^+$ states have been observed.[7,14] Finally, four other Rydberg states (namely, $\tilde{F}'$ 3dδ_g $^1\Phi_u$, $\tilde{H}$ 3dδ_g $^1\Pi_u$, $\tilde{G}$ 4sσ_g $^1\Pi_u$, $\tilde{H}'$ 3dπ_g $^1\Delta_u$) are gathered very close to each other, between 9.91 and 10 eV, justifying the label of 4s−3d supercomplex.[8,11]

Table 3 shows that the *n*d states exhibit small quantum defects, except for the separated lower-lying $\tilde{D}$ 3dσ_g $^1\Pi_u$ and $\tilde{F}$ 3dπ_g $^1\Sigma_u^+$ states. The $\tilde{C}$ 3sσ_g $^1\Pi_u$ and $\tilde{G}$ 4sσ_g $^1\Pi_u$ Rydberg states have a quantum defect close to one. Previous experimental studies have demonstrated the almost pure Rydberg character of the observed higher members of the 4s−3d supercomplex ($\tilde{G}$ $^1\Pi_u$, $\tilde{F}'$ $^1\Phi_u$, and $\tilde{H}'$ $^1\Delta_u$), either by rotationally and vibrationally resolved absorption spectroscopy[8] or by multiphoton photoelectron spectroscopy (REMPI-PES).[10,11,56] On the other hand, two $^1\Pi_u$ Rydberg states ($\tilde{C}$ and $\tilde{H}$) exhibit a very broad absorption profile[5] and could never be detected via REMPI experiments, indicating a very short lifetime.[18]

III.C.1. Analysis of the Lowest ns and nd Rydberg Orbitals. Figure 5 shows the shape of the lowest *n*s and *n*d Rydberg MOs. The external lobes of these orbitals are quasi-hydrogenic, as earlier shown for 3s and 3dσ from SCF calculations.[32] They exhibit a spatial extension following roughly a n^{*2} scaling law, as clearly shown by the 3s and 4s contours. A detailed analysis of the inner parts of the orbitals is clearly required for understanding the penetrating character within the s−d series and to explain the quite large range of quantum defect values (from −0.01 to 0.97) of Table 3.

The 3dδ_g MOs correspond to the simplest case, with pure hydrogenic 3d shapes, explained by the absence of δ_g precursor in the core. The nonpenetrating character is moreover confirmed by the small values of the calculated and observed quantum defects.

On the contrary σ_g Rydberg orbitals are characterized by significant quantum defects (around 0.96 for 3s and 4s and 0.41 for 3dσ_g). These findings are explained by the existence of *real* precursors for these orbitals: the 2σ_g core precursor for the *n*sσ_g MOs and the 3σ_g core precursor for 3dσ_g (see Figure 5).

The situation is more intricate for the 3dπ_g orbitals. One would yet expect similar features for the three states ($^1\Delta_u$, $^1\Sigma_u^-$, and $^1\Sigma_u^+$) arising from the same $(1\pi_u)^3$ $(3d\pi_g)^1$ configuration. With the *virtual* 1π_g precursor, all of these states should be characterized by small quantum defect values. Surprisingly, these expectations hold for the $^1\Delta_u$ and $^1\Sigma_u^-$ states but not for the $^1\Sigma_u^+$ state. The valence 1π_g MO being unoccupied in the wave function, it gives rise to small quantum defect values (−0.08). On the contrary, there is no radial node and no clear precursor signature in the inner part of the 3d ($^1\Sigma_u^+$) MO. At first sight, the shape of this orbital looks like a pure hydrogenic nonpenetrating 3d orbital, although the quantum defect value of 0.3 is far to be negligible. A closer look at Figure 5 shows yet that the 3d ($^1\Sigma_u^+$) MO cannot be superposed on the 3dδ_g

MOs, qualified above as pure hydrogenic orbitals. This point is discussed in the next section in relation with a Rydberg−valence interaction.

III.C.2. $\tilde{F}-\tilde{E}$ Rydberg−Valence Interaction. Experimentally, the $\tilde{D}$ $3d\sigma_g$ $^1\Pi_u$ and $\tilde{F}$ $3d\pi_g$ $^1\Sigma_u^+$ states have been analyzed in detail for three isotopomers of acetylene by Herman and Colin,[7] who found strong spectral perturbations, mostly in the $\tilde{F}$ $3d\pi_g$ $^1\Sigma_u^+$ state. More recently, a PES-REMPI analysis[14] of the $\tilde{D}$, $\tilde{F}$, and $\tilde{E}$ states brought more insight into the underlying Rydberg−valence interaction and into the nature of the $\tilde{E}$ state.

Despite several calculations,[22,25,30,31,35−37] the $\tilde{E}$ valence state has been very poorly characterized theoretically, probably due to rapid configurational changes along the geometry coordinates. Recent ab initio calculations[14] investigated the PES of this valence state of ^1B_u symmetry and gave a strong evidence for a trans-bent geometry for the $\tilde{E}$ state, correlating with the linear $(1\pi_u)^3(1\pi_g)^1$ $^1\Sigma_u^+$ symmetry (see Table 1). Table 2 reports the equilibrium geometry calculated in ref 14 for the $\tilde{E}$ state, with an HCC angle of 161.2° and a minimum energy close to that of the linear $\tilde{F}$ $^1\Sigma_u^+$ Rydberg state. It was demonstrated[14] both theoretically and experimentally that the $\tilde{E}$ and $\tilde{F}$ states undergo a strong Rydberg−valence interaction, responsible for the observed spectral perturbations. Indeed, at the trans-bent equilibrium geometry of the $\tilde{E}$ state, a contribution of the $d\pi$ Rydberg orbital to the $\tilde{E}$ valence state wave function was predicted.[14] The near energetic degeneracy and the very close equilibrium geometries of the trans-bent $\tilde{E}$ valence state and linear $\tilde{F}$ Rydberg state favor a significant and observable mixing between these two states.

Considerations of the Rydberg MOs of acetylene as shown in Figure 5 can add great insight into the mixed Rydberg−valence character of the $\tilde{F}$ state: the $3d\pi_g$ $^1\Sigma_u^+$ orbital exhibits a distorted shape from the hydrogenic case, with the axes of two opposite d lobes being parallel but not collinear, and each of them crossing the *Z*-axis close to one of the carbon atom positions. This distorted shape comes from a constructive mixing of the $3d\pi_g$ hydrogenic orbital with the valence $1\pi_g$ MO. The resulting Rydberg orbital is not simply built from orthogonality with the $1\pi_g$ precursor, and its shape cannot be described by a form like eq 2. The difference comes from the fact that, as pointed out above, the $\tilde{F}$ $^1\Sigma_u^+$ state is mixed with the $\tilde{E}$ singly excited valence state. Its wave function thus contains some admixture of the $(1\pi_u)^3(1\pi_g)^1$ configuration. It follows that the $1\pi_g$ orbital does not play anymore the role of a virtual core precursor like in the other states, but rather that of an occupied orbital which can mix with other orbitals of the same π_g symmetry. Our calculations demonstrate that $1\pi_g$ actually forms a bonding mixing with the $3d\pi_g$ hydrogenic orbital, as shown in Figure 5. The next π_g orbital, occupied by only 0.01 electron in the $\tilde{F}$ Rydberg state wave function, is also drawn in Figure 5. This is the corresponding antibonding orbital which exhibits the expected radial node. Note that we are dealing here with a quite unique case in which the quantum defect does not come from a core precursor, but from a Rydberg−valence mixing inside the outer MO.

III.C.3. Rapid Dissociation of the $\tilde{C}$ State: A Manifestation of Rydbergization in Acetylene. The $\tilde{C}$ $3s\sigma_g$ $^1\Pi_u$ Rydberg state shows an example of Rydbergization of a valence orbital with decreasing R_{C-H} distance, or conversely the transformation of the 3s Rydberg orbital into a valence $6a_1$ orbital along the HCC−H dissociation coordinate, and finally into a 1s type hydrogenic atomic orbital. The concept of Rydbergization was first introduced by Mulliken.[47,48,67]

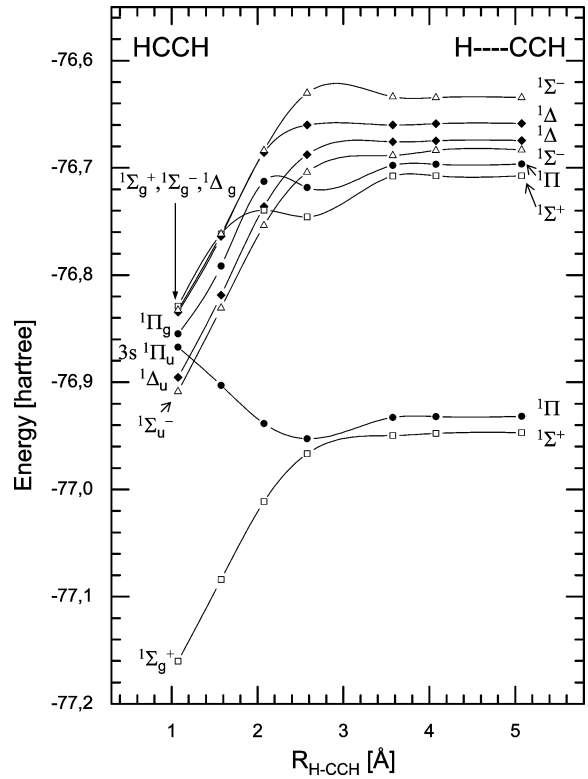

Figure 6. Cut of the CMRCI potential energy surfaces of the ground state and low-lying excited states of acetylene along the CH dissociation coordinate. The symmetries shown to the left of the figure refer to the acetylene states, whereas those to the right correspond to the C_2H fragment states.

Experimentally, it is well-known from the earlier absorption data analyses of Herman and Colin[8] that the lowest Rydberg state, $3s\sigma_g$ $^1\Pi_u$, is strongly predissociated. More recent experiments[28] showed that this state dissociates into the $C_2H(\tilde{A}\ ^2\Pi)$ + H excited channel and that the observed predissociation width is by far larger than that of the other members of the *n*s Rydberg series. The cut of the PES of this state shown in Figure 6 exhibits a rapid decrease along the dissociation coordinate R_{H-CCH} toward the first excited dissociation channel, whereas all the other higher Rydberg states shown in this figure exhibit a greater stability along the same dissociation coordinate. At the centrosymmetric equilibrium geometry, the $3s\sigma_g$ orbital shows an almost pure Rydberg character as displayed in Figure 5. Upon C−H elongation in the linear geometry, this orbital exhibits an increasing valence $6a_1$ character so that, for a C−H bond length of about 5 Å, this orbital becomes of s type, centered on the H atom. At the same distorted geometry, the other outer orbitals converge toward the excited $\tilde{A}$ state configuration of the C_2H fragment.

Other examples of Rydbergization have been reported in the lowest 3s Rydberg states of diatomic hydrides as NH and CH,[48,67] OH,[43,68] and in the isoelectronic N_2 molecule.[48] To our knowledge this is the first quantitative description of such a Rydbergization in a tetra-atomic molecule like C_2H_2 although computational aspects can be found in ref 69.

III.C.4. Rydberg−Rydberg Interaction: Is There an s−d Mixing in Acetylene? ⁄ -Mixing in Rydberg orbitals is a crucial point for understanding the Rydberg spectra of polar molecules, as shown for instance by the extensive work performed by the MIT group of R. W. Field on CaF Rydberg spectra (see for instance ref 70). ⁄ -Mixing in nonpolar Rydberg molecules like NO or N_2 may occur, although to a much less extent, because of the quadrupole field of the ionic

core or because of an s−d mixing in the precursor orbital in the core. For instance, Jungen has shown how the mixed one-center atomic s−d character of the 5σ precursor orbital of the ndσ and (n + 1)sσ Rydberg orbitals is the main responsible (stronger effect than the core quadrupole field) for the strong s−d mixing observed in the Rydberg series of NO.[63] In the N_2 molecule, a similar situation occurs: s−d mixing is observed and mostly ascribed to a similar mixed s−d character of the $3\sigma_g$ precursor orbital of the ndσ and (n + 1)sσ Rydberg orbitals of N_2.[71] It would be interesting to compare with the corresponding sσ and dσ Rydberg orbitals of C_2H_2, isoelectronic with N_2. As shown in Figure 5, the $2\sigma_g$ core orbital is a precursor of the 3sσ and 4sσ molecular orbitals, whereas the $3\sigma_g$ core orbital is the precursor of the 3dσ Rydberg orbital, as in N_2. Unfortunately, a projection of the Rydberg MOs on one-center atomic type orbitals is not easy to extract from the present polyelectronic calculations; therefore the s−d mixing in the $3\sigma_g$ core orbital of acetylene is difficult to quantify. We showed, however, that the $\tilde{C}$ 3s and $\tilde{D}$ 3dσ states are sharing the same electronic configurations built on common state-averaged CASSCF orbitals, whereas the $\tilde{G}$ 4s state exhibits an almost pure s character. This indicates a strong mixing between the 3s and 3dσ Rydberg orbitals and a very weak mixing between the 4s and 3dσ orbitals, unlike in N_2 and NO. This difference with N_2 also appears on the energy scale of the corresponding electronic Rydberg states of C_2H_2 ($\tilde{X}$ $^2\Pi_u$ ionic core) and Rydberg states of N_2 (A $^2\Pi_u$ ionic core). In both molecules the 3dσ Rydberg state lies between the 3s and 4s, but very close to the 4s Rydberg state in the case of N_2, whereas in C_2H_2 the 3dσ state is further apart.

Within the supercomplex formed by the $\tilde{G}$ 4s state and some components of the 3d complex, the $\tilde{H}$ 3dδ state lies very close to the $\tilde{G}$ 4s state (around 160 cm^{-1}). Our calculations also show that there is a very little configuration mixing between the $\tilde{G}$ 4s $^1\Pi_u$ state and $\tilde{H}$ 3dδ $^1\Pi_u$ state.

IV. Conclusion

The present paper extends on several points the previous ab initio approaches[22,25,26,33,36] on the excited singlet Rydberg states of acetylene by means of accurate MRCI calculations:

The Rydberg character including the expected anisotropy of the *n/* Rydberg complexes and scaling laws versus *n** effective principal quantum number, which are widely used in spectroscopic studies, are derived from our results and compared with the experimental data when possible.

Analysis of the Rydberg MOs for all *n*s, *n*p, and *n*d Rydberg states, using very sophisticated and modern ab initio theory, remarkably confirms the very simple Mulliken's ideas stated more than 40 years ago. This analysis has allowed quantizing the Rydberg character of the low-lying observed Rydberg states of acetylene. It happens that most of the Rydberg states follow very well Mulliken's predictions on what concern penetration, anisotropy, and scaling laws. Rydbergization of the 3s orbital of C_2H_2, predicted by Mulliken for diatomic species, has also been theoretically evidenced for the first time.

The observed departure from Rydberg character has been explained by the occurrence of local strong Rydberg−valence interactions, visible on the MO shape, and have been associated with a significant amplitude of the wave function in the core region with or without precursor. For instance, the predissociative character of the 3p and 4p Rydberg states has been quantitatively interpreted as a strong coupling with the $\tilde{C}'$ doubly excited valence state.

Such a multielectronic ab initio calculation is limited to low-lying Rydberg states ($n \leq 5$). For higher Rydberg states, other approaches are more pertinent, such as the multichannel quantum defect theory (MQDT) (see refs 72 and 73 and references therein) or the OVGF approach used in the Zuybin and Mebel work,[26] which builds the description of the Rydberg states from their ionization potential limit. Note that MQDT calculations widely use quantum defects calculated by ab initio methods in low-lying Rydberg states.[71]

The knowledge of the excited PES of the Rydberg states and their interacting valence companion states in the VUV absorbing region remains a challenge in the overall task of the theoretical understanding of the internal dynamics of polyatomic molecules, including dissociation or isomerization.

In particular, this work represents a first step toward a comprehensive study of the isomerization processes in the excited acetylene. Isomerization of excited electronic states has been very poorly investigated both experimentally and theoretically, although it has been proposed to play an important role in the VUV photolysis of acetylene. Indeed, following this photolysis, a large fraction of excited molecules decays into "dark channels".[74] Many hypotheses have been proposed, including isomerization into excited singlet or triplet states of vinylidene. On the other hand, much experimental and theoretical work has been devoted to the ground-state acetylene−vinylidene system which is considered as a prototype for the understanding of the isomerization process in unsaturated hydrocarbons. In particular a pioneering work on the isomerization of the ground state has been carried out for many years by the group of R. W. Field.[1] In a next paper, the valence and Rydberg states of vinylidene will be described at the same level of accuracy as in the present calculation, up to the 10 eV excitation energy region, with the ultimate goal of understanding isomerization processes in excited acetylene.

Acknowledgment. This work was supported by the Wallonie−Bruxelles International and Fonds de la Recherche Scientifique, by the Ministère Français des Affaires étrangères et européennes, and Ministère de l'Enseignement Supérieur et de la Recherche under the Hubert Curien programme partnership "TOURNESOL" no. 18084. J.L. gratefully acknowledges Paris-Sud 11 University for a 1 month invited professorship. He also thanks the Fonds National de la Recherche Scientifique (FNRS, contracts FRFC and IISN) and the "Action de Recherches Concertées de la Communauté française de Belgique" for financial support. M. G. Destrée is acknowledged for his efficient help for solving computational problems.

References and Notes

(1) Jacobson, M. P.; Field, R. W. *J. Phys. Chem. A* **2000**, *104*, 3073.
(2) Glassgold, A. E. *Annu. Rev. Astron. Astrophys.* **1996**, *34*, 241.
(3) Herbst, E. *Chem. Soc. Rev.* **2001**, *30*, 168.
(4) Herbst, E. *J. Phys. Chem. A* **2005**, *109*, 4017.
(5) Suto, M.; Lee, L. C. *J. Chem. Phys.* **1984**, *80*, 4824.
(6) Han, J. C.; Ye, C.; Suto, M.; Lee, L. S. *J. Chem. Phys.* **1989**, *90*, 4000.
(7) Herman, M.; Colin, R. *J. Mol. Spectrosc.* **1981**, *85*, 449.
(8) Herman, M.; Colin, R. *Phys. Scr.* **1982**, *25*, 275.
(9) Ashfold, M. N. R.; Tutcher, B.; Yang, B.; Jin, Z. K.; Anderson, S. L. *J. Chem. Phys.* **1987**, *87*, 5105.
(10) Orlando, T.; Anderson, S. L.; Appling, J. R.; White, M. G. *J. Chem. Phys.* **1987**, *87*, 852.
(11) Fillion, J. H.; Campos, A.; Pedersen, J.; Shafizadeh, N.; Gauyacq, D. *J. Chem. Phys.* **1996**, *105*, 22.
(12) Shafizadeh, N.; Fillion, J. H.; Gauyacq, D.; Couris, S. *Philos. Trans. R. Soc. London, Ser. A* **1997**, *355*, 1637.
(13) Campos, A.; Boyé, S.; Douin, S.; Fellows, C.; Fillion, J. H.; Shafizadeh, N.; Gauyacq, D. *J. Phys. Chem. A* **2001**, *105*, 9104.
(14) Blanchet, V.; Boyé, S.; Zamith, S.; Campos, A.; Girard, B.; Liévin, J.; Gauyacq, D. *J. Chem. Phys.* **2003**, *119*, 3751.
(15) Hsu, Y. C.; Lin, M. S.; Hsu, C. P. *J. Chem. Phys.* **1991**, *94*, 7832.
(16) Cool, T.; Goldwin, P. *J. Chem. Phys.* **1991**, *94*, 6978.
(17) Wang, J.-H.; Hsu, Y.-T.; Liu, K. *J. Phys. Chem. A* **1997**, *101*, 6593.

(18) Löffler, P.; Wrede, E.; Schnieder, L.; Halpern, J. B.; Jackson, W. M.; Welge, K. H. *J. Chem. Phys.* **1998**, *109*, 5231.

(19) Löffler, P.; Lacombe, D.; Ross, A.; Wrede, E.; Schnieder, L.; Welge, K. H. *Chem. Phys. Lett.* **1996**, *252*, 304.

(20) Boyé, S.; Campos, A.; Douin, S.; Fellows, C.; Gauyacq, D.; Shafizadeh, N.; Halvick, P.; Boggio-Pasqua, M. *J. Chem. Phys.* **2002**, *116*, 8843.

(21) Qian, X. M.; Kung, A.; Ng, C. Y. *Abstr. Pap.—Am. Chem. Soc.* **2003**, *225*, U478.

(22) Peric, M.; Buenker, R. J.; Peyerimhoff, S. D. *Mol. Phys.* **1984**, *53*, 1177.

(23) Liévin, J. *J. Mol. Spectrosc.* **1992**, *156*, 123.

(24) Halvick, P.; Liotard, D.; Rayez, J. C. *Chem. Phys.* **1993**, *177*, 69.

(25) Malsch, K.; Rebentisch, R.; Swiderek, P.; Hohlneicher, G. *Theor. Chem. Acc.* **1998**, *100*, 171.

(26) Zyubin, A. S.; Mebel, A. M. *J. Chem. Phys.* **2003**, *119*, 6581.

(27) Nakayama, T.; Watanabe, K. *J. Chem. Phys.* **1964**, *40*, 558.

(28) Campos, A.; Boyé, S.; Bréchignac, P.; Douin, S.; Fellows, C.; Shafizadeh, N.; Gauyacq, D. *Chem. Phys. Lett.* **1999**, *314*, 91.

(29) Kammer, W. E. *Chem. Phys. Lett.* **1970**, *6*, 529.

(30) Kammer, W. E. *Chem. Phys.* **1974**, *5*, 408.

(31) Demoulin, D. *Chem. Phys.* **1975**, *11*, 329.

(32) Peyerimhoff, S. D.; Buenker, R. J. In *Chemical Spectroscopy and Photochemistry in the Vacuum-Ultraviolet. Proceedings of the Advanced Study Institute, NATO and Royal Society of Canada*; Sandorfy, C., Ausloos, P. J., Robin, M. B., Eds.; D. Reidel: Dordrecht/Boston, 1973; Vol. 8, p 257.

(33) Peric, M.; Peyerimhoff, S. D. In *Understanding Chemical Reactivity—The Role of Rydberg States in Spectroscopy and Photochemistry. Low and High Rydberg States*; Sandorfy, C., Ed.; Kluwer Academic Publishers: Dordrecht/Boston/London, 1999; Vol. 20, p 137.

(34) Demoulin, D.; Jungen, M. *Theor. Chim. Acta* **1974**, *34*, 1.

(35) Peric, M.; Peyerimhoff, S. D.; Buenker, R. J. *Mol. Phys.* **1985**, *55*, 1129.

(36) Peric, M.; Peyerimhoff, S. D.; Buenker, R. J. *Mol. Phys.* **1987**, *62*, 1339.

(37) Lischka, H.; Karpfen, A. *Chem. Phys.* **1986**, *102*, 77.

(38) Wetmore, R. W.; Schaefer, H. F., III. *J. Chem. Phys.* **1978**, *69*, 1648.

(39) So, S. P.; Wetmore, R. W.; Schaefer, H. F., III. *J. Chem. Phys.* **1980**, *73*, 5706.

(40) (a) Stanton, J. F.; Huang, C.-M.; Szalay, P. G. *J. Chem. Phys.* **1994**, *101*, 356. (b) Cui, Q.; Morokuma, K.; Stanton, J. F. *Chem. Phys. Lett.* **1996**, *263*, 46.

(41) Cui, Q.; Morokuma, K. *Chem. Phys. Lett.* **1997**, *272*, 319.

(42) Li, J.; Liu, Y.; Dai, X.; Li, L.; Field, R. W. *J. Chem. Phys.* **2001**, *114*, 7859.

(43) Lefebvre-Brion, H.; Field, R. W. *The Spectra and Dynamics of Diatomic Molecules*; Elsevier Academic Press: Amsterdam/Boston/Heidelberg/London/New York/Oxford/Paris/San Diego/San Francisco/Singapore/Sidney/Tokyo, 2004.

(44) Duncan, A. B. F. In *Rydberg Series in Atoms and Molecules, Physical Chemistry*; Loebl, E. M., Ed.; Academic Press: New York/London, 1971; Vol. 23.

(45) *Rydberg States of Atoms and Molecules*; Stebbings, R. F., Dunning, F. B., Eds.; Cambridge University Press: Cambridge, 1983.

(46) *Understanding Chemical Reactivity—The Role of Rydberg States in Spectroscopy and Photochemistry. Low and High Rydberg States*; Sandorfy, C., Ed.; Kluwer Academic Publishers: Dordrecht/Boston/London, 1999; Vol. 20.

(47) Mulliken, R. S. *J. Am. Chem. Soc.* **1964**, *86*, 3183.

(48) Mulliken, R. S. *Acc. Chem. Res.* **1976**, *9*, 7.

(49) Werner, H.-J.; Knowles, P. J.; Lindh, R.; Manby, F. R.; Schütz, M.; Celani, P.; Korona, T.; Rauhut, G.; Amos, R. D.; Bernhardsson, A.; Berning, A.; Cooper, D. L.; Deegan, M. J. O.; Dobbyn, A. J.; Eckert, F.; Hampel, C.; Hetzer, G.; Lloyd, A. W.; McNicholas, S. J.; Meyer, W.; Mura, M. E.; Nicklass, A.; Palmieri, P.; Pitzer, R.; Schumann, U.; Stoll, H.; Tarroni, R.; Thorsteinsson, T. MOLPRO, 2006.1 ed., 2006.

(50) Werner, H.-J.; Knowles, P. J. *J. Chem. Phys.* **1988**, *89*, 5803.

(51) Knowles, P. J.; Werner, H.-J. *Chem. Phys. Lett.* **1985**, *115*, 259.

(52) (a) Woon, D. E.; Dunning, T.-H. *J. Chem. Phys.* **1995**, *103*, 4572. (b) Dunning, T.-H. *J. Chem. Phys.* **1989**, *90*, 1007.

(53) Dunning, T. H.; Hay, P. J. In *Methods of Electronic Structure Theory*; Schaefer, H. H., III, Ed.; Plenium Press: New York/London, 1977; p 1.

(54) Langhoff, S. R.; Davidson, E. R. *Int. J. Quantum Chem.* **1974**, *8*, 62.

(55) Shaftenaar, G.; Noordik, J. H. *J. Comput.-Aided Mol. Des.* **2000**, *14*, 123.

(56) Ashfold, M. N. R.; Dixon, R. N.; Prince, J. D.; Tutcher, B. *Mol. Phys.* **1985**, *56*, 1185.

(57) Takahashi, M.; Fujii, M.; Ito, M. *J. Chem. Phys.* **1992**, *96*, 6486.

(58) Tsuji, K.; Arakawa, N.; Kawai, A.; Shibuya, K. *J. Phys. Chem. A* **2002**, *106*, 747.

(59) Ingold, C. K.; King, G. W. *J. Chem. Soc.* **1953**, 2702.

(60) Foo, P. D.; Innes, K. K. *Chem. Phys. Lett.* **1973**, *22*, 439.

(61) Lundberg, J. K.; Jonas, D. M.; Rajaram, B.; Chen, Y.; Field, R. W. *J. Chem. Phys.* **1992**, *97*, 7180.

(62) Lundberg, J. K.; Chen, Y.; Picque, J.-P.; Field, R. W. *J. Chem. Phys.* **1992**, *156*, 104.

(63) Jungen, C. *J. Chem. Phys.* **1970**, *53*, 4168.

(64) Matthiasson, K.; Wang, H.; Kvaran, A. *Chem. Phys. Lett.* **2008**, *458*, 58.

(65) Walsh, A. D. *J. Chem. Soc.* **1953**, 2288.

(66) Buenker, R. J.; Peyerimhoff, S. D. *Chem. Phys. Lett.* **1975**, *36*, 415.

(67) Mulliken, R. S. *Chem. Phys. Lett.* **1972**, *14*, 141.

(68) Lefebvre-Brion, H. *J. Mol. Struct.* **1973**, *19*, 103.

(69) Kassab, E.; Evleth, E. M. In *Understanding Chemical Reactivity—The Role of Rydberg States in Spectroscopy and Photochemistry. Low and High Rydberg States*; Sandorfy, C., Ed.; Kluwer Academic Publishers: Dordrecht/Boston/London, 1999; Vol. 20, p 231.

(70) Field, R. W.; Gittins, C. M.; Harris, N. A.; Jungen, C. *J. Chem. Phys.* **2005**, *122*, 184314.

(71) Raoult, M.; Le Rouzo, H.; Raseev, G.; Lefebvre-Brion, H. *J. Phys. B: At. Mol. Opt. Phys.* **1983**, 16.

(72) Jungen, C.; Atabek, O. *J. Chem. Phys.* **1977**, *66*, 5584.

(73) Greene, C. H.; Jungen, C. *Adv. At. Mol. Phys.* **1985**, *21*, 51.

(74) Satyapal, S.; Bershon, R. *J. Phys. Chem.* **1991**, *95*, 8004.

(75) Dressler, R.; Allan, M. *J. Chem. Phys.* **1987**, *87*, 4510.

(76) Boyé-Péronne, S.; Gauyacq, D.; Liévin, J. *J. Chem. Phys.* **2006**, *124*, 214305.

(77) Rupper, P.; Merkt, F. *Rev. Sci. Instrum.* **2004**, *75*, 613.

JP903948K